JCTC Journal of Chemical Theory and Computation

Article

pubs.acs.org/JCTC

Peak-Shifting in Real-Time Time-Dependent Density Functional Theory

Makenzie R. Provorse, Bradley F. Habenicht, and Christine M. Isborn*

Chemistry and Chemical Biology, University of California Merced, Merced, California 95343, United States

Supporting Information

ABSTRACT: In recent years, the development and application of real-time time-dependent density functional theory (RT-TDDFT) has gained momentum as a computationally efficient method for modeling electron dynamics and properties that require going beyond a linear response of the electron density. However, the RT-TDDFT method within the adiabatic approximation can unphysically shift absorption peaks throughout the electron dynamics. Here, we investigate the origin of these time-dependent resonances observed in RT-TDDFT spectra. Using both exact exchange and hybrid exchange-correlation approximate functionals, adiabatic RT-TDDFT gives time-dependent absorption spectra in which the peaks shift in energy as populations of the excited states fluctuate, while exact wave function methods yield peaks that are constant in energy but vary in intensity. The magnitude of the RT-TDDFT peak shift depends on the frequency and intensity of the applied field, in line with previous studies, but it oscillates as a function of time-dependent molecular orbital populations, consistent with a time-dependent superposition electron density. For the first time, we provide a rationale for the direction and magnitude of the time-dependent peak shifts based on the molecular electronic structure. For three small molecules, H_2, HeH^+, and LiH, we give contrasting examples of peak-shifting to both higher and lower energies. The shifting is explained as coupled one-electron transitions to a higher and a lower lying state. Whether the peak shifts to higher or lower energies depends on the relative energetics of these one-electron transitions.

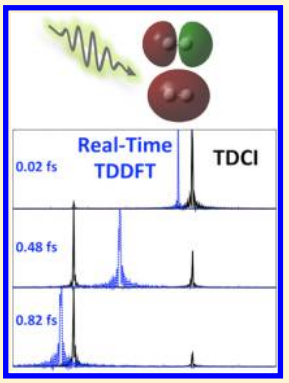

1. INTRODUCTION

In the past decade, time-dependent density functional theory (TDDFT) has become the method of choice for the calculation of the valence excited states of large molecules.[1−4] The linear response (LR) limit of TDDFT has a straightforward matrix formulation that computes frequency domain excitation energies of the ground state density and has been implemented in many electronic structure packages.[5] LR-TDDFT has been used to model such diverse systems as dye-sensitized solar cells,[6] helicene molecules,[7] and nanoparticles[8] to list just a few. Although TDDFT with standard approximate functionals has well-documented problems, such as difficulties describing Rydberg transitions[9] and charge-transfer transitions being too low in energy,[10] much effort is being dedicated to improve this method.[11,12]

In real-time time-dependent density functional theory (RT-TDDFT), the density $n(\mathbf{r},t)$ of noninteracting electrons evolves in time and at all points in time must be identical to the exact time-dependent fully interacting many-body electron density. When the electron density is subject to an external perturbation, the time-dependent density may be used to extract the observables as a function of time.[5] Since the RT-TDDFT method evolves the electronic density in the time-domain, it can easily take into account a time-dependent external electric field.[13−16] The exchange-correlation (XC) potential should be a functional of the time-dependent density $n(\mathbf{r},t)$ as well as the initial interacting wave function and noninteracting Kohn−Sham single-particle molecular orbitals (MOs); thus, it is a functional of not only the initial wave function but also the density at all points in time (i.e., it has a history dependence via a "memory" of the past density).[17−23] In practice, approximate ground state functionals are used within the adiabatic approximation for both LR and RT applications. In most implementations of RT-TDDFT, the instantaneous density is inserted into a ground state functional, even though the time-dependent density may be significantly different from the ground state density.

Because of its ability to model the electronic response of a molecule to specific time-dependent fields and pulses, RT-TDDFT has the potential to simulate electron dynamics when a short-time (atto- or femtosecond) laser field is applied to a system, which would be of great use in explaining the results of various pump−probe experiments and time-resolved spectroscopic observables.[16] In addition, RT-TDDFT can explicitly model time-dependent phenomena such as charge-transfer and exciton dynamics in donor−acceptor molecules applicable to the development of solar cells,[24−26] molecular conductance,[27] and plasmon behavior in noble metal nanowires and nanoparticles.[28,29] RT-TDDFT has also been used to predict ideal field intensities and frequencies to induce cross-linking between amino acid residues[30] and to model excited state absorption.[31] The method can be easily combined with Ehrenfest dynamics to include the nuclear response to an applied field.[32−34] This

Received: June 15, 2015
Published: September 4, 2015

ACS Publications © 2015 American Chemical Society

DOI: 10.1021/acs.jctc.5b00559
J. Chem. Theory Comput. 2015, 11, 4791−4802

method can also be coupled to classical force fields and continuum solvent models to include solvent effects on spectroscopic observables.[35−38]

RT-TDDFT naturally includes the response of the electron density beyond the linear response regime. If the applied field does not significantly perturb the ground state electron density, Fourier transform of the oscillations of the RT-TDDFT dipole moment reproduces electronic transitions predicted by LR-TDDFT.[39−41] However, at high field intensities, RT-TDDFT includes the response of the electron density to all orders, not just LR, and has been used to model the nonlinear optical properties of polyenes.[39,42] Additionally, when a large number of states in the absorption spectrum are desired, the standard LR matrix formulation may be computationally intractable. In RT-TDDFT the entire spectrum is obtained from a single Fourier transform, so it can be more computationally efficient than solving for many eigenvalues of the LR-TDDFT matrix.[43]

Despite its growing popularity, fundamental aspects of RT-TDDFT and consequences of its practical implementation have been questioned. As with time-independent DFT and LR-TDDFT, RT-TDDFT is formally an exact method given that the exact XC contribution to the potential is known. Because most applications of RT-TDDFT rely on the adiabatic approximation in which only the instantaneous electron density is used with a ground state functional, the dependence of the XC functional on the history of the density and initial states is neglected. Recent work by Maitra and co-workers derives an exact condition from which it follows that the exact XC functional must include memory-dependent and cancel the time-dependence of the response frequencies.[44] Because of the approximate nature of the XC functional within the adiabatic approximation, RT-TDDFT electron dynamics may differ substantially from the correct result as the density is driven away from the ground state.[45−49]

One substantial problem is how RT-TDDFT with approximate time-independent XC functionals treats resonant excitations. Applying a field that is resonant with the frequencies predicted by LR theory generally does not excite the electron density to the appropriate excited state.[15,45,47−49] This behavior makes it impossible to use adiabatic RT-TDDFT to correctly model laser-induced excitation processes or Rabi oscillations. Although Rabi oscillations may be induced with a strong enough field, the population oscillations involve two electrons instead of the expected single-electron process, and the field frequency is not what was expected from LR theory.[15,49] This phenomenon is connected to RT-TDDFT having resonant frequencies that depend on the time-dependent reference state.[48] The RT-TDDFT equations are nonlinear since the two-electron terms in the potential, Coulomb and exchange-correlation, depend on the time-dependent electron density, which leads to a dynamic potential. Within the adiabatic approximation, this leads to an unphysical time-dependent electronic structure, which will be dependent on the applied electric field and how much the field has perturbed the density away from the ground state reference.[40,41,50−53] According to work by Maitra and co-workers,[44] the memory-dependence of the exact XC functional should yield a time-independent electronic structure by exactly canceling these time-dependent resonances. It is rationalizing these problematic time-dependent resonances of adiabatic RT-TDDFT to which we turn our attention in this article.

The lack of memory within the adiabatic approximation leads to spurious peak-shifting in the absorption and emission spectrum when a molecule is excited from its ground reference state.[54] Nest and co-workers examined molecular systems, including LiCN and Li_2C_2, and found that peaks shift to higher energies as a function of the energy absorbed by the system, which is directly related to the intensity of the applied field.[51,52] Molecular symmetry and small changes in the magnitude and orientation of the permanent dipole upon excitation were identified as desirable molecular properties for reliable RT-TDDFT results.[51,53] Recently, Fischer et al. have modeled excited state absorption using RT-TDDFT starting from a LR excited state density.[31] They have also observed peaks shifted from the expected values. To the best of our knowledge, neither the direction nor the magnitude of peak-shifting in RT-TDDFT spectra have been explained.

In order to better understand adiabatic RT-TDDFT electron dynamics, we here investigate the origin of the time-dependent peak-shifting found in RT-TDDFT spectra by comparing RT-TDDFT with exact wave function results for simple, two-electron molecules: H_2 and HeH^+. We recently studied these systems by RT-TDDFT in the context of inducing Rabi oscillations,[48] in which it was found that population oscillation between the bonding and antibonding orbitals was dependent on both the frequency and intensity of the applied electric field. In our previous work we used only a minimal basis set for simplicity of analysis within a two-level system. Here we extend that analysis to a larger basis set and a multielectron molecule and show that our explanation of the peak-shifting is the same for these more complicated systems.

Overall, we find that for RT-TDDFT the energy of the peaks in an absorption spectrum depends on the time-dependent MO occupations based on projection of the time-dependent density matrix on to the initial MOs. Using these time-dependent MO populations, we explain both the magnitude and direction of the peak-shifting in the RT-TDDFT spectrum. When the time-dependent density populates two MOs of different symmetry (σ and σ^*), the time-dependent resonance corresponds to coupled single-electron transitions. These transitions must be uncoupled to create physically correct time-independent resonances.

2. COMPUTATIONAL METHODS

In this section we briefly review the theory of RT-TDDFT and give the relevant computational details. Readers are referred to ref 13 for the full description of the RT-TDDFT implementation. RT-TDDFT is a time domain method for propagating the time-dependent electron density. The TDDFT equation, using the electron density $\mathbf{P}(t)$ and the Kohn−Sham/Fock matrix, $\mathbf{F}(t)$, may be written as (atomic units [$\hbar = e = m_e = 1$] are used unless stated otherwise)

$$i\frac{\partial \mathbf{P}(t)}{\partial t} = [\mathbf{F}(t), \mathbf{P}(t)] \tag{1}$$

Here the Kohn−Sham matrix is time-dependent not only from the time-dependent field but also because the electron−electron interaction potential (both Coulomb and exchange-correlation) depends on the time-dependent density. This is in contrast to the exact Hamiltonian, which is time-independent when the field is removed. In our calculations, we use the standard adiabatic approximation to the exchange-correlation functional, in which there is no dependence on the density at previous points in time, the dependence of the functional on the initial fully interacting wave function and the noninteracting

DOI: 10.1021/acs.jctc.5b00559
J. Chem. Theory Comput. 2015, 11, 4791−4802

Kohn−Sham wave function is ignored, and only the instantaneous time-dependent electron density is used with a ground state functional to determine the energetics of the electron response.

The modified midpoint algorithm[13] evolves the electron density matrix **P** from time t_{m-1} to time t_{m+1}

$$\mathbf{P}(t_{m+1}) = \mathbf{U}(t_m)\mathbf{P}(t_{m-1})\mathbf{U}^{\dagger}(t_m) \quad (2)$$

.

Here, **U** is a unitary transformation matrix that is formed with the eigenvectors ($\mathbf{c}(t_m)$) and eigenvalues ($\varepsilon(t_m)$) obtained by diagonalizing the Kohn−Sham/Fock matrix

$$\mathbf{U}(t_m) = \mathbf{c}(t_m)\exp[i\varepsilon(t_m)2\Delta t]\mathbf{c}^{\dagger}(t_m) \quad (3)$$

where Δt is the time step of the simulation. To monitor the evolution of the system, the time-dependent density matrix $\mathbf{P}(t)$ is projected on the $t = 0$ eigenvectors, which are the initial MO coefficients, giving the populations $N(t)$ of the MOs as

$$N_i(t) = c_i^{\dagger}(0)\mathbf{P}(t)c_i(0) \quad (4)$$

Since RT-TDDFT does not have formally defined states, this projection of the density matrix onto the $t = 0$ MOs is used to analyze the evolution of the electron density.[13] While our analysis relates these Kohn−Sham MO populations to populations of electronic states, this procedure should be performed with caution. Population of the Kohn−Sham MOs that represent the system of noninteracting electrons may be significantly different than the population of the states in the interacting system. Additionally, the population of electronic states may correspond to population of multiple virtual MOs. While the MO analysis is fairly simple for the minimal basis set, it does indeed become more complicated for the larger 6-31G basis.

For the first set of RT-TDDFT results presented here, full exact Hartree−Fock (HF) exchange was used for the exchange functional, and no correlation was included, in which case the RT-TDDFT results are identical to RT-TDHF. Similar peak-shifting results are obtained with the B3LYP functional[55,56] as explained later in the paper. To start, we use a minimal basis set, STO-3G, such that H_2 and HeH^+ are pseudo-two-level systems. Expanding our study to a larger basis, 6-31G, we obtain similar trends in peak-shifting but find the spectra are significantly more complicated because there are several higher lying states that can be populated and will contribute to the superposition electron density. For LiH with the STO-3G basis, all four electrons are active in the RT electron dynamics.

For comparison, we also ran time-dependent configuration interaction (TDCI)[13,39] simulations of the same systems. Full CI calculations provide input for the TDCI simulations, including energetics and transition dipole moments for the doubly excited states not available in standard LR-TDDFT calculations. For full CI in the minimal basis set, each state is dominated by a single configuration; we can therefore relate population of that state to population of the corresponding MO. With the larger basis set, more configurations contribute to each state, which complicate the analysis, and we discuss the state in the context of the configuration with the largest coefficient. Full CI of LiH includes over 100 configurations which becomes computationally expensive when state-averaging. Thus, the Li 1s core electrons were not included in the CI and a (2,5) active space with equal weighting of all 15 states through state-averaging was used to compute the CI transition energies and transition dipole moments of LiH.

The LR-TDDFT, RT-TDDFT, and CI calculations were performed using the Gaussian development version.[57] The CI results were then used in our python implementation of TDCI, based on Mathematica notebooks provided by Berny Schlegel.[13,39] RT-TDDFT and TDCI electron dynamics used a time step of 0.002 and 0.05 fs, respectively. In each simulation, an electric field was applied in the z-direction along the molecular bond (see Table S1 for field parameters). Both TDCI and RT-TDDFT methods use the dipole approximation to couple the field to the molecule, with the field modeled as a simple sine function. After the electric field was turned off, the dipole moment was allowed to oscillate field-free for 12 fs. The final 10 fs of the z-component of the field-free dipole moment was Fourier transformed to obtain absorption spectra. The total energy of each simulation was conserved to within 2×10^{-5} hartree once the field was removed. Due to oscillations in the RT-TDDFT density even after the applied field is turned off, all expectation values will oscillate with respect to time. To account for oscillations in the projected MO populations, the average MO population is computed from the last 500 steps of each simulation. Throughout this paper, "MO population" refers to this average MO population value.

For the TDCI approach, it is straightforward to apply a resonant field, or sequential resonant fields, to excite the system to a specific state. However, this is not the case with RT-TDDFT due to the problem with time-dependent resonant excitations.[44,49] The field frequencies for the RT-TDDFT population inversion are not the frequencies obtained from a LR calculation using the ground state reference, and we have found that using a field frequency that is approximately an average of the LR response excitation energy and the energy for de-excitation from the doubly excited state will cause population transfer.[49] Increasing the field intensity broadens the range of frequencies around the average that yield full population transfer. Various field frequencies and intensities are used throughout this work to populate specific MOs corresponding to the excited states of interest. In the Supporting Information (SI), we have details of the specific fields used for both the TDCI and RT-TDDFT simulations described in this work.

For the simple minimal basis calculations on two-electron molecules, a single field frequency can excite both electrons to nearly fully populate the higher energy MO. Since the electronic structure is more complicated with the larger basis set, the field will generally excite the density to multiple states, and it is difficult to obtain an MO population that directly corresponds to a specific state. In these cases, we resort to a Koopmans' excitation of the electrons directly into MOs rather than starting the simulation from the converged ground state density, as noted in the text.

3. RESULTS AND DISCUSSION

3.1. H_2 and HeH^+ Using a Minimal Basis with Exact Exchange. H_2 and HeH^+ are simple, two-electron systems that allow us to compare RT-TDDFT peak-shifting in a symmetric and an asymmetric molecule with equivalent electronic structure. In a minimal basis, these molecules are modeled by two MOs with bonding (σ) and antibonding (σ^*) character and have three possible electronic states, each dominated by a single electronic configuration: two electrons in σ (S_0), one electron in each orbital (S_1), and two electrons in σ^* (S_2). CI

DOI: 10.1021/acs.jctc.5b00559
J. Chem. Theory Comput. 2015, 11, 4791−4802

transition dipole moments indicate that H_2 has only two allowed transitions in this minimal basis: $S_0 \rightarrow S_1$ and $S_1 \rightarrow S_2$ (Table 1). HeH^+ has an additional allowed transition, $S_0 \rightarrow S_2$,

Table 1. Transition Energies (hartree) and Transition Dipole Moments (Debye) of H_2 and HeH^+ Computed Using a Minimal STO-3G Basis[a]

molecule	method	$\Delta E_{S_0 \rightarrow S_1}$	$\Delta E_{S_1 \rightarrow S_2}$	$\mu_{zS_0 \rightarrow S_1}$	$\mu_{zS_1 \rightarrow S_2}$
H_2	CI	0.98	0.66	1.16	1.45
	LR/HF	0.94		1.19	
	LR/B3LYP	0.94		1.18	
HeH^+	CI	0.83	1.34	0.89	0.46
	LR/HF	0.90		0.84	
	LR/B3LYP	0.84		0.86	

[a]The molecular bond is oriented along the z-axis. The energy and properties of the doubly excited S_2 state are not accessible via linear response TDDFT/TDHF.

although the oscillator strength is very small ($f = 0.07$). We will show that the relative energies of the $S_0 \rightarrow S_1$ and $S_1 \rightarrow S_2$ single-electron energy gaps lead to RT-TDDFT absorption peaks that shift in opposite directions for these two molecules. In this section we use full exact exchange with the Hartree–Fock (HF) functional to avoid self-interaction error; therefore, the peak-shifting is not an artifact of self-interaction.

With a small field perturbation, the density remains close to the ground state, and the RT-TDDFT spectrum agrees with the LR excitation energies obtained from using the same ground state density as a reference. When an electric field of the appropriate strength and frequency is applied to H_2 or HeH^+ (see the SI for specific field parameters), RT-TDDFT yields significant population inversion between the σ and σ^* MOs, indicating that the RT-TDDFT electron density is a superposition density that oscillates between double occupation of σ and σ^*.[48,49] Figure 1 shows the RT-TDDFT populations of the

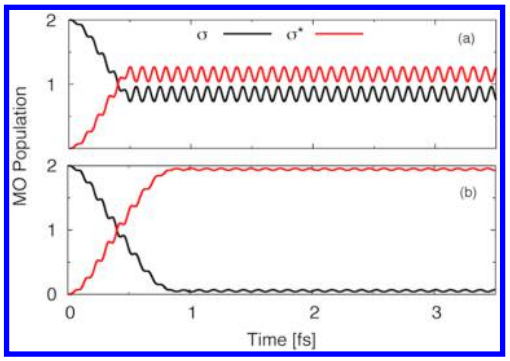

Figure 1. Populations of the bonding σ and antibonding σ^* MO of H_2 from RT-TDDFT STO-3G simulations for field durations of (a) 0.48 fs and (b) 0.82 fs calculated using eq 4. The final superposition state is determined by the pulse length of the applied field.

σ and σ^* MOs for H_2 at two different field durations. Starting from the converged ground state density with both electrons in the σ MO and applying the field for 0.48 fs gives a population of ~1 electron in each MO (top panel), and a longer field duration of 0.82 fs gives a population of ~2 electrons in the σ^* MO (bottom panel). Note that the electron density is restricted to a singlet state (i.e., restricted HF), requiring the α and β spatial symmetry to be the same at all times in the dynamics. Similar results for HeH^+ are obtained with a field applied for 0.36 and 0.76 fs (Figure S1).

TDCI simulations produce similar results by sequentially applying two fields with frequencies resonant with the $S_0 \rightarrow S_1$ and $S_1 \rightarrow S_2$ transition energies (Table 1). The first field is applied for 0.68 fs to give full population of the S_1 state (Figure 2). Then a second field is applied for 0.64 fs to give full

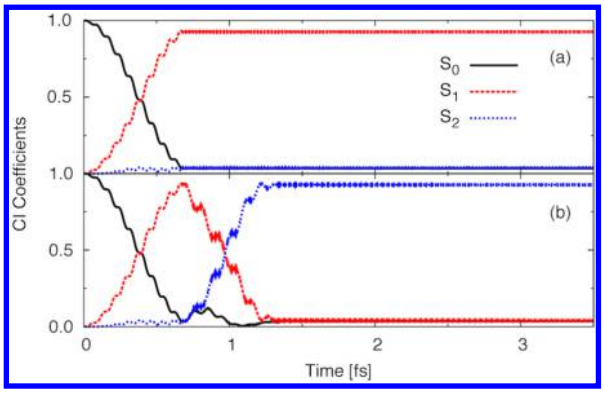

Figure 2. CI coefficients of H_2 from TDCI STO-3G simulations that populate the (a) S_1 and (b) S_2 excited states.

population of the S_2 state. As expected, the MO occupations rise and fall during the TDCI simulation according to the time-dependent state populations. Similar TDCI results are obtained for HeH^+ by applying a field for 0.31 fs and a second field for 0.89 fs (Figure S2). In agreement with previous studies,[49] the frequencies used in the TDCI simulations correspond to CI $S_0 \rightarrow S_1$ and $S_1 \rightarrow S_2$ transition energies (Table 1) but differ from the frequencies used in RT-TDDFT simulations (Table S1) to induce $\sigma \rightarrow \sigma^*$ MO population transfer.

Figure 3 shows the TDCI and RT-TDDFT absorption spectra for H_2 with populations of zero, one, and two electrons

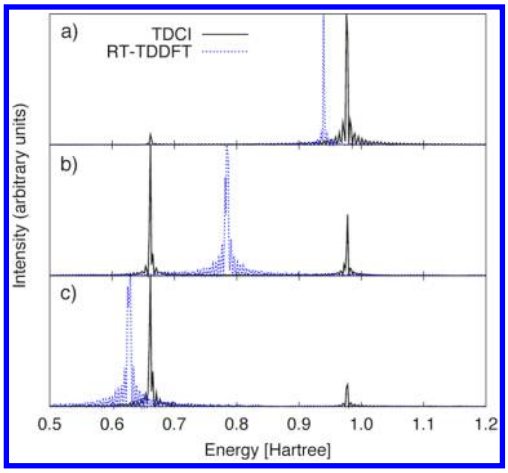

Figure 3. TDCI (exact) and RT-TDDFT spectra of H_2 for a) population of two electrons in σ, b) population of one electron in σ and one electron in σ^*, and c) population of two electrons in σ^*. Spectra are normalized to the most intense peak.

in the σ^* MO, given by the field parameters described above. Note that the intensities of the peaks in the spectra change according to TDCI state populations and RT-TDDFT MO populations, as expected, but each spectrum is normalized to the tallest peak for ease of comparison. TDCI simulations (solid black) show two peaks that correspond to the $S_0 \rightarrow S_1$

DOI: 10.1021/acs.jctc.5b00559
J. Chem. Theory Comput. 2015, 11, 4791–4802

and $S_1 \rightarrow S_2$ transition energies at 0.98 and 0.66 hartree, respectively. Depending on the state population, the peaks have different intensities but remain at a constant energy, i.e. they display a time-independent electronic structure. When starting from the ground state electron density, the RT-TDDFT peak (dashed blue) is at the frequency predicted by LR-TDDFT of 0.94 hartree (Figure 3a). This is in good agreement with the CI $S_0 \rightarrow S_1$ transition energy of 0.98 hartree (Table 1). However, this RT-TDDFT resonance is time-dependent and the RT-TDDFT spectra portray qualitatively different behavior than TDCI: for RT-TDDFT there is only one peak, and this peak shifts between the $S_0 \rightarrow S_1$ and $S_1 \rightarrow S_2$ transition energies. When the electron density fully populates σ^* (Figure 3c), the peak energy is similar to the CI $S_1 \rightarrow S_2$ transition energy of 0.66 hartree (Table 1). Thus, for TDCI the *intensity* of the peaks change based on the electronic state of the system, but for RT-TDDFT the *intensity and energy* of a single peak changes as the electron density propagates in time.

Figure 4 shows how the intensity of the field affects the RT-TDDFT MO population and resulting peak energy. When the

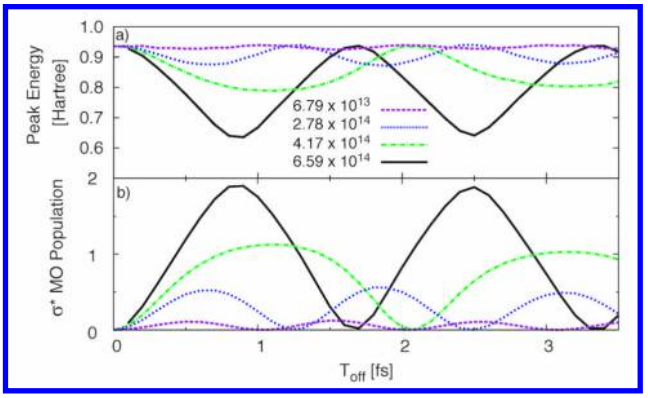

Figure 4. a) Peak energy and b) σ^* MO population eq 4 as a function of the applied field pulse length (T_{off}) for a series of RT-TDDFT simulations of H_2 with a frequency of 0.78 hartree increasing field intensity (W/cm^2).

σ MO is fully populated, i.e. very close to the ground state electron density, the peak is at the frequency predicted by LR-TDDFT. However, as the intensity of the applied field increases the peak shifts to *lower* energy as electron density is moved to the σ^* orbital. Figure 4 shows that while the field remains on, the electron density moves back to the ground state and the peak energy shifts back to the LR value. The electron density and peak energy continue to oscillate as a function of the pulse length, despite the additional energy pumped into the system. Higher intensity fields shorten the Rabi oscillation frequency rather than increasing the magnitude of the peak shift (Figure S3).

For HeH^+, there is a small but finite transition dipole moment between S_0 and S_2, resulting in three peaks in the TDCI spectrum corresponding to the $S_0 \rightarrow S_1$, $S_1 \rightarrow S_2$, and $S_0 \rightarrow S_2$ transitions at 0.83, 1.34, and 2.17 hartree, respectively (see Figure 5 and Table 1). Similar to the H_2 results, for any point in the TDCI dynamics, these peaks shift in intensity but remain at a constant energy. RT-TDDFT electron dynamics again predicts a single peak in the spectrum that agrees with the LR transition energy in the ground state (Figure 5a) but oscillates in energy between the $S_0 \rightarrow S_1$ and $S_1 \rightarrow S_2$ transition energies. In contrast to H_2, the HeH^+ peak shifts to *higher*

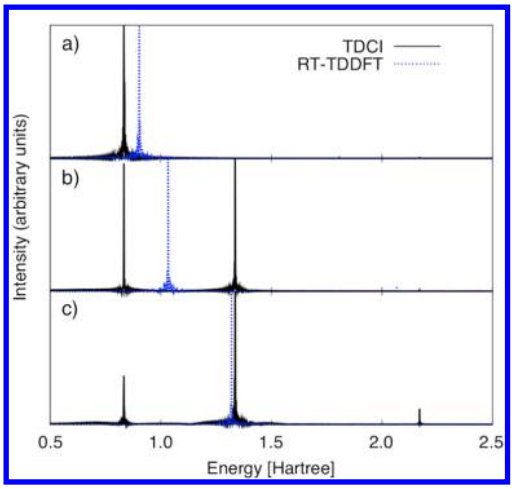

Figure 5. Simulated TDCI and RT-TDDFT spectra of HeH^+ for a) population of two electrons in σ, b) population of one electron in σ and one electron in σ^*, and c) population of two electrons in σ^*. All spectra are normalized to the most intense peak.

energy as the σ^* MO becomes more populated (Figure 6), and the magnitude of the HeH^+ peak shift is larger than the H_2 peak

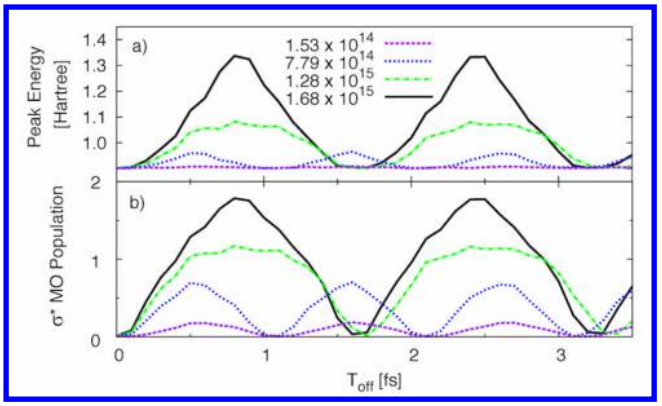

Figure 6. a) Peak energy and b) σ^* MO population eq 4 as a function of the applied field pulse length (T_{off}) from a series of RT-TDDFT simulations of HeH^+ with a frequency of 1.04 hartree and increasing field intensity (W/cm^2).

shift. As with H_2, fields with intensities above the threshold intensity do not induce larger peak shifts but instead shorten the Rabi oscillation frequency.

How can we rationalize the direction and magnitude of the observed peak shifts for H_2 and HeH^+? If we could use the exact XC functional beyond the adiabatic approximation, there would be no unphysical peak-shifting. However, the exact XC functional is unknown, so instead we compare the RT-TDDFT results to the full CI exact transition energies, which provide information about the S_2 state not available in LR-TDDFT calculations. From the TDCI spectra, we see that as the S_2 state is populated, the dominant one-electron transition becomes the $S_1 \rightarrow S_2$ transition. For H_2 and HeH^+, the relative energies of the $S_0 \rightarrow S_1$ and $S_1 \rightarrow S_2$ transitions differ. For H_2, the CI $S_0 \rightarrow S_1$ transition energy is larger than the $S_1 \rightarrow S_2$ transition (Table 1), so the RT-TDDFT peak energy shifts down in energy as the electron density increasingly represents the S_2 state (i.e., double occupation of σ^*). For HeH^+, the opposite is true; the $S_1 \rightarrow S_2$ transition energy is larger than the $S_0 \rightarrow S_1$ transition. As a consequence, the RT-TDDFT peak energy shifts up in energy

DOI: 10.1021/acs.jctc.5b00559
J. Chem. Theory Comput. 2015, 11, 4791−4802

as the electron density increasingly represents the S_2 state. This behavior is further shown in Figure 7 where the peak energy is

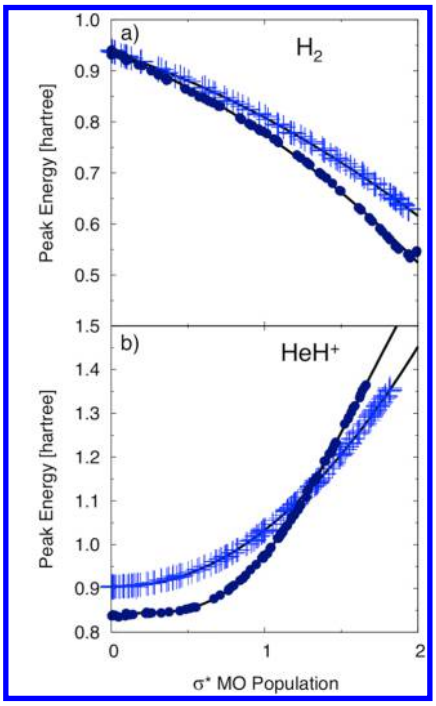

Figure 7. Peak energy as a function of σ^* MO population for H_2 and HeH^+ using full exact exchange with TDHF (cross) and TDB3LYP (circle). Black lines are quadratic functions fit to the initial increase in σ^* MO population from 0 to ~2 electrons.

plotted as a function of σ^* orbital occupation for H_2 (top panel) and HeH^+ (bottom panel). The peak energy shifts in opposite directions for H_2 and HeH^+, in agreement with relative one-electron transition energies of each system. Also, the magnitude of the peak shift is larger for HeH^+ because the $S_0 \rightarrow S_1$ and $S_1 \rightarrow S_2$ transition energies differ by 0.51 hartree for HeH^+ compared to only 0.32 hartree for H_2. Note the maximum σ^* MO population of HeH^+ is smaller than that of H_2 because MO populations of HeH^+ tend to oscillate to a greater degree than H_2 (Figure S1). The solid black lines shown in Figure 7 are quadratic functions fit to the first half of the first Rabi oscillation cycle of each molecule. The peak energies from all subsequent Rabi oscillations agree with the values predicted by the initial increase in σ^* MO population of each molecule.

Based on the correlation shown in Figure 7 between peak energy and σ^* MO population, we infer that within the adiabatic approximation, the electron density is a superposition of S_0 and S_2 states at all times during RT-TDDFT dynamics. The applied electric field perturbs the ground state density to a superposition of S_0 and S_2 densities and the resulting peak energy is a superposition of the $S_0 \rightarrow S_1$ and $S_1 \rightarrow S_2$ transition energies weighted by the relative contribution of S_0 and S_2 to the superposition density. We here see that by not including the functional dependence on the initial wave function and the history dependence of the density, single-electron transitions become coupled when Kohn–Sham MOs become partially occupied. Here we do not mean that the transitions are "coupled" in the sense of multiple Kohn–Sham MO single-electron transitions contributing to one state-to-state transition, but we mean "coupled" in that the time-dependent resonance represents two different transitions that are coupled by the evolving time-dependent density. We therefore propose that in addition to making the electronic resonances time-independent as shown by Maitra and co-workers,[44] the exact XC functional must uncouple the transitions that represent simultaneous single-electron excitation and de-excitation out of the two populated Kohn–Sham MOs.

We have chosen to study H_2 and HeH^+ not only because of their simple electronic structure but also because they provide a direct comparison of symmetric and asymmetric molecules with and without permanent dipole moments, respectively. Nest and co-workers suggested that systems that are symmetric along the axis parallel to the applied field exhibit smaller peak shifts than asymmetric molecules[51] and that molecules with larger differences between the permanent dipole moment in the ground and excited states lead to larger peak shifts.[51,53] Here, we find that asymmetric HeH^+ does in fact give a larger peak shift in energy than H_2, but this is not due to the symmetry of the molecule or the presence of a nonzero dipole moment. Instead, our analysis shows that for both H_2 and HeH^+ the direction and magnitude of the observed peak shift from RT-TDDFT simulations is determined by the relative $S_0 \rightarrow S_1$ and $S_1 \rightarrow S_2$ one-electron transition energies. This rationale for the direction and magnitude of the peak-shifting is further supported in section 3.3 where H_2 is modeled by a larger basis, giving rise to superposition of multiple one-electron transitions.

Nest and co-workers also attribute the magnitude of peak shifts to the amount of energy supplied to the system.[51,52] Our analysis refutes this claim based on three observations: (i) at long pulse lengths the peak energy remains within the $S_0 \rightarrow S_1$ and $S_1 \rightarrow S_2$ one-electron transition energies (Figures 4 and 6), (ii) at field intensities above the Rabi threshold intensity the magnitude of the peak shift does not increase (Figures S3), and (iii) the amount of energy absorbed by the system, defined as the difference between the initial and final total energy of a simulation, oscillates as a function of the applied field pulse length for a given field intensity (Figure S4). Despite additional energy pumped into the system, either by allowing the field to stay on longer or using a stronger field, the peak energy does not continue to increase. In fact, the peak energy decreases with increasing energy absorbed by H_2 (Figure S5). Thus, the direction and maximum magnitude of the peak shift is determined by the difference between the $S_0 \rightarrow S_1$ and $S_1 \rightarrow S_2$ one-electron transition energies. The degree of the peak shift is determined by how much the electron density has been perturbed by the applied field, not how much energy has been supplied to the system.

3.2. H_2 and HeH^+ Using a Minimal Basis with B3LYP Exchange-Correlation. Before we investigate a larger basis in the next section, we first examine the effects of correlation by replacing the HF functional with B3LYP, an approximate hybrid exchange-correlation density functional.[55,56] Figure 7 shows the RT-TDDFT peak energy as a function of σ^* occupation computed using the B3LYP functional using field parameters similar to those described in the previous section. The direction of the peak shift is reproduced for each system, where H_2 shifts *down* in energy and HeH^+ shifts *up* in energy as electron density increasingly populates the σ^* orbital. The magnitude of the peak shift is increased for both molecules. For H_2, the initial, unperturbed density gives a peak energy of 0.93 hartree (Figure 7), in agreement with the LR-TDDFT excitation energy computed using B3LYP (Table 1). When σ^* is doubly occupied the RT-TDB3LYP peak energy (0.54

DOI: 10.1021/acs.jctc.5b00559
J. Chem. Theory Comput. 2015, 11, 4791–4802

Table 2. Transition Energies (hartree) and Transition Dipole Moments (Debye) of H_2 Computed Using a 6-31G Basis Set[a]

method	$\Delta E_{\sigma\to\sigma^*}$	$\Delta E_{\sigma'\to\sigma^*}$	$\Delta E_{\sigma\to 2\sigma^*}$	$\Delta E_{\sigma'\to 2\sigma^*}$	$\mu_{z,\sigma\to\sigma^*}$	$\mu_{z,\sigma'\to\sigma^*}$	$\mu_{z,\sigma\to 2\sigma^*}$	$\mu_{z,\sigma'\to 2\sigma^*}$
LR	0.56		1.62		1.32		−0.25	
CI	0.56	0.56	1.77	1.34	1.29	1.47	−0.17	−0.05
	$\Delta E_{\sigma^*\to 2\sigma}$	$\Delta E_{\sigma^{*\prime}\to 2\sigma}$	$\Delta E_{2\sigma\to 2\sigma^*}$	$\Delta E_{2\sigma'\to 2\sigma^*}$	$\mu_{z,\sigma^*\to 2\sigma}$	$\mu_{z,\sigma^{*\prime}\to 2\sigma}$	$\mu_{z,2\sigma\to 2\sigma^*}$	$\mu_{z,2\sigma'\to 2\sigma^*}$
	0.30	0.54	0.66	0.48	−1.24	−0.95	−1.24	−1.57

[a]The molecular bond is oriented along the z-axis. The energy and properties of the doubly excited S_2 state are not accessible via linear response TDDFT/TDHF. A prime indicates the initial MO is singly occupied.

hartree) is smaller than the RT-TDHF exact exchange peak energy (0.63 hartree). This suggests that the $S_1 \to S_2$ energy gap is smaller for TDB3LYP than TDHF; thus, the difference between the $S_0 \to S_1$ and $S_1 \to S_2$ transition energies is larger for TDB3LYP than with TDHF. For HeH^+, LR TDB3LYP predicts a smaller $S_0 \to S_1$ transition energy (0.84 hartree) than LR TDHF exact exchange (0.90 hartree), in better agreement with the CI $S_0 \to S_1$ transition energy (Table 1), but RT TDB3LYP appears to give a similar $S_1 \to S_2$ transition energy (1.33 hartree). Therefore, in both systems, the difference between the $S_0 \to S_1$ and $S_1 \to S_2$ transition energies is larger using TDB3LYP than TDHF, resulting in a larger peak shift.

3.3. H_2 Using the 6-31G Basis with Exact Exchange. In this section H_2 is modeled using the 6-31G basis set and exact HF exchange. This basis set is still relatively small (an additional s-orbital is added to each atom), so we do not expect the excitation energies to be converged to the basis set limit. However, increasing the basis set size to 6-31G allows us to investigate peak-shifting in systems with more complicated electronic structure by introducing two additional higher lying MOs. We show that although the absorption spectra become more complicated with a larger basis, the rationale for the peak-shifting remains the same as with a minimal basis: the energies shift as a function of MO population corresponding to multiple one-electron transitions between orbitals.

The 6-31G basis gives four MOs for H_2, where the two additional virtual orbitals have bonding and antibonding character and are labeled here as 2σ and $2\sigma^*$. Full CI with this larger basis has eight allowed one-electron transitions. Transitions between these states are dominated by configurations with one electron moving between the following MOs: $\sigma \to \sigma^*$, $\sigma \to 2\sigma^*$, $\sigma^* \to 2\sigma$, and $2\sigma \to 2\sigma^*$. Each of these MO combinations corresponds to two CI state transitions with different initial MO occupations. For example, the $\sigma \to \sigma^*$ transition in the minimal basis corresponds to both $S_0 \to S_1$ and $S_1 \to S_2$ transitions, with the first transition initially having two electrons in σ, and the second initially having one electron in σ. Here, we denote a transition from an initially singly occupied orbital with a prime ($'$), while transitions without a prime are initially from a doubly occupied orbital, so that the $\sigma \to \sigma^*$ and $\sigma' \to \sigma^*$ transitions are equivalent to the minimal basis $S_0 \to S_1$ and $S_1 \to S_2$ transitions, respectively. The CI and LR TDHF transition energies and transition dipole moments are given in Table 2.

As with the minimal basis, a small perturbation gives spectral peaks at energies that agree with a LR response calculation. To obtain peaks shifted from the LR values, we must significantly perturb the density from the ground state and populate the higher lying MOs. The peak-shifting analysis is more complicated for the RT-TDDFT simulations with the larger basis set because, in addition to more peaks shifting in the absorption spectrum, it is difficult to find field parameters that cleanly populate only two MOs. Because this is not a simple two-level system, we did not find a frequency that yields Rabi population inversion between two MOs, and we therefore could not fit the peak energies to populations of the first part of a Rabi cycle as was done in Figure 7. Instead, the peak-shifting is analyzed in the context of two MOs being mostly populated (below 0.1e- in any of the other MOs), but the small population of the other MOs leads to some scatter in the peak energies. Regardless, we show that, as with the smaller basis, the peak energy correlates with MO occupations and can be rationalized in terms of coupled single-electron transitions. Applying an electric field for 0.25 fs moves ∼1 electron from σ to σ^*, while applying the same field for 1.65 fs increases that to ∼2 electrons in σ^* and nearly zero in the σ orbital (Figure 8). The high-

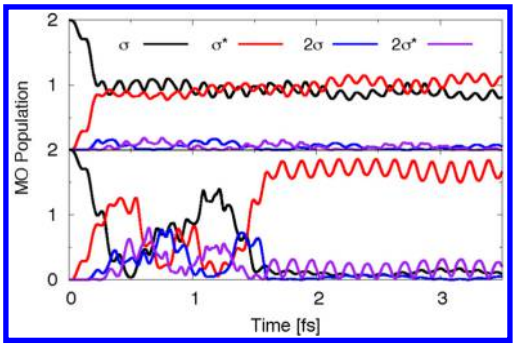

Figure 8. Populations of the bonding σ and 2σ and the antibonding σ^* and $2\sigma^*$ MOs of H_2 from RT-TDDFT 6-31G simulations with exact exchange for field durations of 0.25 fs (top panel) and 1.65 fs (bottom panel).

energy 2σ and $2\sigma^*$ orbitals gain considerable occupation (∼0.9 electron) at specific pulse lengths, but their occupation is nearly zero when the σ and σ^* orbital occupations are at their respective minima and maxima (Figure S6). We will first focus on the $\sigma \to \sigma^*$ and $\sigma' \to \sigma^*$ peak shifts that correspond to the $S_0 \to S_1$ and $S_1 \to S_2$ minimal basis transitions examined in Section 3.1 and then analyze other peaks that correspond to population of the higher energy MOs.

Choosing applied field pulse lengths that predominantly induce population transfer from σ to σ^* (less than 0.1 electron in each of the 2σ and $2\sigma^*$ orbitals), the RT-TDDFT absorption spectrum is dominated by a single peak at ∼0.5 hartree. Figure 9a shows that as electron density moves from σ to σ^* the peak energy shifts from 0.55 to 0.51 hartree. For clarity, the σ population is not shown in Figure 9a, but this data is available in the Supporting Information (Figure S7a). The peak energy near zero σ^* population is in agreement with the corresponding LR ground to excited state $\sigma \to \sigma^*$ transition energy of 0.56 hartree (Table 2). The CI transition energy between excited states that corresponds to a $\sigma' \to \sigma^*$ one-electron transition happens to also be 0.56 hartree; thus, no peak shift would be observed if the TDDFT energies agree with the CI energies.

DOI: 10.1021/acs.jctc.5b00559
J. Chem. Theory Comput. 2015, 11, 4791−4802

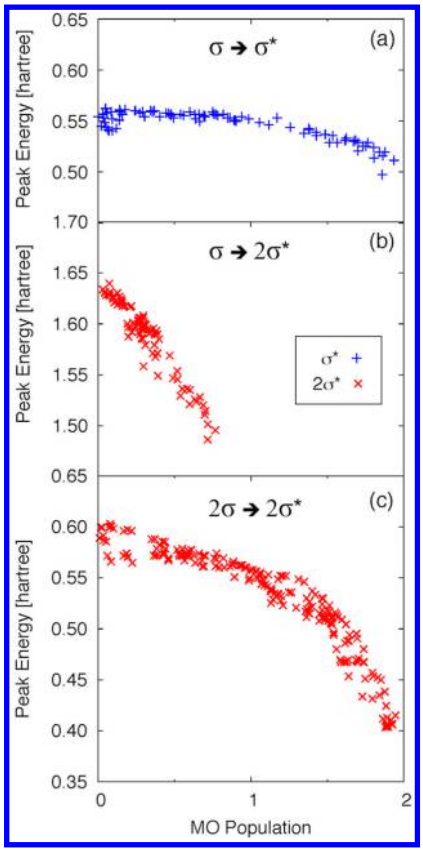

Figure 9. Peak energy as a function of σ^* or $2\sigma^*$ MO population corresponding to population transfers (a) $\sigma \rightarrow \sigma^*$, (b) $\sigma \rightarrow 2\sigma^*$, and (c) $2\sigma \rightarrow 2\sigma^*$ from RT-TDDFT simulations of H_2 using 6-31G basis and exact exchange.

However, the RT-TDDFT peak shifts down in energy by 0.04 hartree as σ^* population increases to ∼2 electrons.

It is expected that RT-TDDFT peak energies may be slightly different than the CI transition energies, but to confirm that a RT-TDDFT peak energy near 0.51 hartree corresponds to a doubly occupied σ^*, field-free RT-TDDFT simulations were carried out using a Koopmans' type excitation to give an initial electron density with ∼2 electrons in σ^*. This field-free RT-TDDFT simulation gave a peak at 0.50 hartree; thus, we are confident that the 0.55 to 0.51 hartree peak shift shown in Figure 9a corresponds to the superposition of one-electron transitions $\sigma \rightarrow \sigma^*$ and $\sigma' \rightarrow \sigma^*$, as was rationalized with the minimal basis $S_0 \rightarrow S_1$ and $S_1 \rightarrow S_2$ transitions in Section 3.1.

We focus next on the high-energy peak that corresponds to a ground to excited state transition dominated by a one-electron transition between $\sigma \rightarrow 2\sigma^*$. The LR energy for this transition is 1.62 hartree, and the corresponding CI transition is slightly higher in energy at 1.77 hartree. The CI excited state to excited state transition dominated by a $\sigma' \rightarrow 2\sigma^*$ one-electron transition occurs at 1.32 hartree, while if we perform a Koopmans' excitation to doubly occupy $2\sigma^*$, the field-free RT-TDDFT high-energy peak is at 1.42 hartree. Thus, using a similar rationale as with the previous peak-shifting analysis, we would expect the RT-TDDFT peak to shift from 1.62 hartree to 1.42 hartree as the $2\sigma^*$ MO becomes doubly occupied. While no field parameters that we tried gave complete double-electron population of $2\sigma^*$, the same field parameters that predominately give the $\sigma \rightarrow \sigma^*$ transition also shift the population of approximately one electron from σ to $2\sigma^*$. Figure 9b shows that increasing population of $2\sigma^*$ correlates with a decrease in peak energy from 1.64 to 1.49 hartree. The peak energy shifts only halfway between the transition energies predicted by LR and field-free RT-TDDFT simulations of the doubly occupied $2\sigma^*$ density because only ∼1 electron is transferred. Note the increase in $2\sigma^*$ MO population mirrors a decrease in σ MO population (Figure S7b), indicating a $\sigma \rightarrow 2\sigma^*$ transition.

In the RT-TDDFT spectrum, lower energy peaks in the 0.3 to 0.6 hartree range are also observed that have no counterpart in the LR calculation. These presumably correspond to transitions between excited states that are not obtained when using the ground state as a reference in the LR calculation. The CI transition energies suggest that peaks in this energy range are related to the $\sigma^* \rightarrow 2\sigma$ and $2\sigma \rightarrow 2\sigma^*$ transitions. To isolate the $2\sigma \rightarrow 2\sigma^*$ transition, we used Koopman excitations to obtain initial electron densities corresponding to doubly occupied 2σ and $2\sigma^*$ orbitals; field-free RT-TDDFT simulations on these densities gave maximum intensity peaks at 0.60 and 0.40 hartree, respectively. Applying an electric field to a doubly occupied 2σ density induces significant MO population transfer to $2\sigma^*$ (∼1.40 electrons), while applying a field to a doubly occupied $2\sigma^*$ density induces ∼1.25 electron transfer to 2σ. Figure 9c includes data points from both of these simulations, where the higher-energy peak of the two most intense peaks from the 2σ simulation and the most intense peak from the $2\sigma^*$ simulation are plotted as a function of $2\sigma^*$ orbital occupation. As expected based on the MO population analysis, the peak energy decreases from 0.60 to 0.40 hartree as electron density is transferred from 2σ to $2\sigma^*$ (see Figure S7c for corresponding decrease in 2σ MO population). In addition, a decrease in peak energy with increasing $2\sigma^*$ MO occupation is consistent with a smaller CI $2\sigma' \rightarrow 2\sigma^*$ than $2\sigma \rightarrow 2\sigma^*$ transition energy (Table 2).

Unfortunately, the peak shift corresponding to the $\sigma^* \rightarrow 2\sigma$ transition was not isolated since the field frequencies applied to both the doubly occupied σ^* and 2σ densities induced significant MO population transfer into and out of all four orbitals. This suggests that the remaining peak shifts correspond to superpositions of multiple one-electron transitions and thus cannot be analyzed in this simple manner.

3.4. H_2 and HeH^+ RT-TDDFT Dynamics Starting from the LR S_1 State. Instead of starting the RT-TDDFT electron dynamics from a converged ground state density as discussed previously, we here apply the perturbation to the S_1 excited state density obtained from a LR calculation, as has been previously done by Fischer et al. for modeling excited state absorption.[31] These excited state densities are obtained by solving a Z-vector equation.[58,59] Running a RT-TDDFT simulation on the LR S_1 density of H_2 with a very small perturbation gives a single peak at 0.80 hartree, which agrees with the RT-TDDFT peak energy the population of each MO is approximately 1 (Figure 7a). Similarly, a RT-TDDFT simulation applying a small perturbation to the LR S_1 density of HeH^+ using a minimal basis and exact exchange gives a single peak at 1.05 hartree. This agrees with the RT-TDDFT peak energy when the population of each MO of HeH^+ is ∼1 electron (Figure 7b). For both H_2 and HeH^+ with a minimal basis, two single-electron transition peaks would be expected from the S_1 state (one corresponding to excitation to S_2 and another to de-excitation to the ground S_0 state at the energy given by LR theory); thus, a single peak shifted in energy confirms that RT-TDDFT in the adiabatic approximation will

DOI: 10.1021/acs.jctc.5b00559
J. Chem. Theory Comput. 2015, 11, 4791−4802

couple single-electron transitions. The result is also consistent with the fractional MO occupations that correlate with a single peak that oscillates between the $S_0 \rightarrow S_1$ and $S_1 \rightarrow S_2$ transition energies.

Using the 6-31G basis, RT-TDDFT simulations that apply a small perturbation to the LR S_1 density of H_2 gives three low energy peaks at 0.48, 0.54, and 0.57 hartree and a high energy peak at 1.59 hartree. The 0.54 hartree peak agrees with Figure 9a when population of the σ and σ^* MOs is each ~1 electron, indicating that this peak corresponds to the coupled single-electron transitions for de-excitation to the ground state and excitation to the doubly excited state. The peak at 0.48 hartree agrees with the CI $\sigma^* \rightarrow 2\sigma$ transition at 0.48 hartree, and the high energy peak at 1.59 hartree is similar in energy to the 1.56 hartree CI a $\sigma \rightarrow 2\sigma^*$ transition. We were able to isolate this latter transition and corresponding peak shift using RT-TDDFT simulations starting from the ground state density (see Section 3.3). This agreement with the CI energies suggests that RT-TDDFT is capable of modeling resonances between excited states when starting from a LR excited state density.

3.5. LiH Using a Minimal Basis with Exact Exchange. To expand our peak-shifting analysis to molecules with more than two electrons, four-electron LiH is modeled with the STO-3G basis set using exact HF exchange. In this minimal basis, LiH consists of 6 MOs. Given in order of increasing energy, they are: Li 1s, bonding σ, Li 2s with some σ bonding character, Li $2p_x$ and $2p_y$, and an antibonding σ^* orbital. In the RT-TDDFT simulations, an electric field is applied along the molecular axis of LiH in the z-direction; thus, negligible electron density moves into the nonbonding Li $2p_x$ and $2p_y$ orbitals perpendicular to the applied field. However, starting from the ground state, we are able populate the Li 2s or the σ^* MO with minimal population of the other virtual MOs (Figure 10a and b), which results in peak-shifting with less scatter than was seen for H_2 with the 6-31G basis set. We focus here on the time-dependent resonances corresponding to population transfer between the following MOs: $\sigma \rightarrow$ Li 2s and $\sigma \rightarrow \sigma^*$ (Figure 10c). The CI and LR TDHF transition energies and transition dipole moments that are dominated by the following one-electron transitions are given in Table 3: $\sigma \rightarrow$ Li 2s, $\sigma' \rightarrow$ Li 2s, $\sigma \rightarrow \sigma^*$, and $\sigma' \rightarrow \sigma^*$, where a prime indicates single occupation of the MO.

For RT-TDDFT, applying a small perturbation to the ground state density gives peaks at energies corresponding to the LR $\sigma \rightarrow$ Li 2s and $\sigma \rightarrow \sigma^*$ transition energies of 0.17 and 0.63 hartree. When the virtual MOs become populated, additional peaks appear in the spectrum that correspond to transitions between excited states, but these peaks are not analyzed here. Applying an electric field to populate the Li 2s MO (see SI for all field parameters) transfers ~0.6e- from σ to Li 2s (Figure 10a). This population change causes the lower energy peak to shift up in energy from 0.17 to 0.25 hartree (Figure 10c, blue squares), while the higher energy peak corresponding to the coupled $\sigma \rightarrow \sigma^*$ and $\sigma' \rightarrow \sigma^*$ transitions does not shift in energy. Extrapolation of the trend shown in Figure 10c (blue squares) to ~2e- population of the Li 2s MO predicts a peak near 0.46 hartree. The initial peak energy of 0.17 hartree and the extrapolated peak energy of 0.46 hartree are in good agreement with the CI calculation, which predicts an excitation energy from the ground state of 0.14 hartree (corresponding to a $\sigma \rightarrow$ Li 2s one-electron transition) and a de-excitation energy of 0.44 hartree (corresponding to a Li 2s $\rightarrow \sigma'$ one-electron transition) (Table 3). Thus, the RT-TDDFT peak shifting to higher energies (from 0.17 to 0.46 hartree) for this multi-electron molecule is consistent with our previous analysis of coupled single-electron transitions.

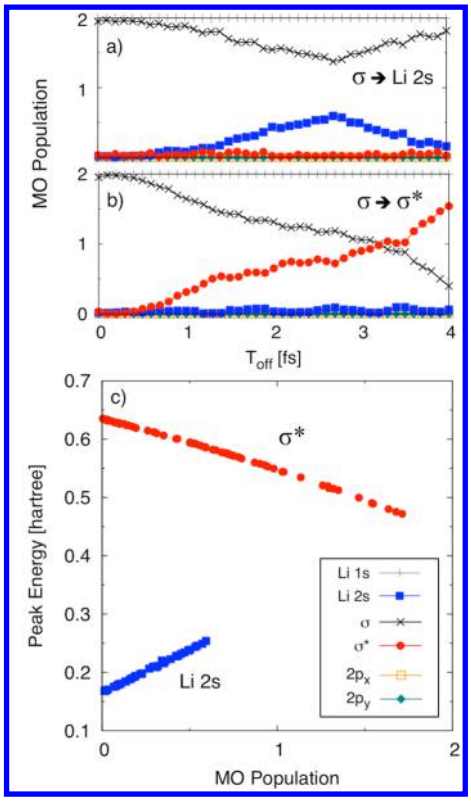

Figure 10. MO populations from RT-TDDFT simulations of LiH using the minimal basis and exact exchange: different field frequencies are used to induce a) $\sigma \rightarrow$ Li 2s and b) $\sigma \rightarrow \sigma^*$ population transfer. Corresponding peak energies are shown in c) as a function of Li 2s and σ^* MO population.

Using different field parameters, population is transferred from σ to σ^* (Figure 10b) and the higher energy peak, which agrees with the LR $\sigma \rightarrow \sigma^*$ transition energy of 0.63 hartree (Table 3), shifts down in energy from 0.63 to 0.47 hartree (Figure 10c, red circles). These peak energies again are in good agreement with the CI calculation which predicts a ground to excited state transition dominated by $\sigma \rightarrow \sigma^*$ at 0.68 hartree and a de-excitation energy of 0.45 hartree for a transition dominated by $\sigma^* \rightarrow \sigma'$ (Table 3). Note that the lower energy peak corresponding to the $\sigma \rightarrow$ Li 2s transition remains constant in energy as population transfers to the σ^* MO. The behavior of these RT-TDDFT resonances remains consistent with our analysis and is due to different reference densities: the peak shifting to lower energies (from 0.63 to 0.47 hartree) corresponds to a coupled single-electron excitation/de-excitation as the reference density transfers population between σ and σ^*, while the peak at 0.17 hartree, corresponding to the $\sigma \rightarrow$ Li 2s transition, remains constant as density transfers into σ^* because the reference density does not transfer population into the Li 2s MO.

With our study of RT-TDDFT peak-shifting in LiH, we can explain why one peak shifts to lower energies and one to higher energies in terms of coupled single-electron transitions. Also, we see the important example of a peak *not shifting* when the reference density does not contain any contribution from an excited state coupled to that peak. Our rationale for the direction and magnitude of the time-dependent resonances

DOI: 10.1021/acs.jctc.5b00559
J. Chem. Theory Comput. 2015, 11, 4791−4802

Table 3. Transition Energies (hartree) and Transition Dipole Moments (Debye) of LiH Computed Using a Minimal STO-3G Basis Set[a]

method	$\Delta E_{\sigma\to\sigma^*}$	$\Delta E_{\sigma'\to\sigma^*}$	$\Delta E_{\sigma\to \mathrm{Li}2s}$	$\Delta E_{\sigma'\to \mathrm{Li}2s}$	$\mu_{z\sigma\to\sigma^*}$	$\mu_{z\sigma'\to\sigma^*}$	$\mu_{z\sigma\to \mathrm{Li\ 2s}}$	$\mu_{z\sigma'\to \mathrm{Li\ 2s}}$
LR	0.63		0.17		0.82		−0.49	
CI	0.68	0.45	0.14	0.44	−1.33	0.49	−0.73	−0.04

[a]The molecular bond is oriented along the z-axis. The energy and properties of excited states with double occupation of the σ^* or Li 2s MO are not accessible via linear response TDDFT/TDHF. Additional CI transitions are not shown. A prime indicates the initial MO is singly occupied.

thus holds for a multielectron molecule. We expect the same peak-shifting behavior for larger, more complicated molecular systems; however, our analysis approach may not be appropriate if multiple transitions are overlapping in energy or if multiple virtual MOs become occupied from the perturbation.

4. CONCLUSIONS

In this article, nonphysical peak-shifting previously reported for RT-TDDFT within the adiabatic approximation is systematically investigated using simple molecular systems. By applying an electric field of appropriate intensity and frequency, the ground state electron density is significantly perturbed. Fourier transform of the resulting dipole moment gives absorption peaks that shift in energy as the reference density is driven away from the ground state and higher lying states become populated. Using H_2 and HeH^+ as contrasting examples, we show that the direction and magnitude of RT-TDDFT peak shifts are explained in terms of coupled one-electron transition energies, one corresponding to excitation and one to de-excitation. With the simple MO picture of H_2 and HeH^+ in the minimal basis, the peak energy shifts from a resonance corresponding to a one-electron excitation out of a doubly occupied σ orbital to a one-electron de-excitation out of a doubly occupied σ^* orbital. This is consistent for both exact exchange and the B3LYP functional and also holds true regardless of molecular symmetry, excited state symmetry, or presence of a molecular dipole moment. Our rationale is extended to more complicated electronic structures with H_2 in a 6-31G basis and LiH with a minimal basis. For more realistic systems that have the possibility of electron excitation into many more states, it may be difficult to fully populate a single virtual MO; instead many higher lying MOs may have small occupations. These small occupations would lead to peak-shifting that is smaller in magnitude than that studied here when a virtual MO becomes fully populated with two electrons.

Using the excited state density from a LR response calculation as a starting point for a RT-TDDFT calculation yields absorption peaks shifted to the same energy obtained from a RT-TDDFT calculation that excites the ground state electron density to equally populate two MOs. For H_2 and HeH^+ in the minimal basis, it might be expected that two peaks would appear in the spectrum when starting from the LR excited state density - one peak corresponding to single-electron absorption and another corresponding to single-electron emission. Instead we observe a single peak at a value 0.14 hartree lower than the emission energy that would be predicted by LR theory. From our analysis, this peak is due to the coupling of single-electron transitions from the two occupied MOs, resulting in a single peak at an energy that is the average of the two coupled transition energies.

Overall, our analysis shows that using RT-TDDFT while perturbing a molecule significantly away from the ground state density will lead to time-dependent resonances that shift in energy according to coupled single-electron transitions between two occupied MOs. The shift will occur to either higher or lower energy depending on the relative energies of the coupled single-electron transitions. This unphysical phenomenon will lead to incorrect field-dependent resonances when simulating highly perturbed electron dynamics and will also lead to incorrect rates of electron transfer between states. The RT-TDDFT method must therefore be used with great caution when moving beyond the ground state electron density.

This work highlights the need for improved density-functional approximations that go beyond the adiabatic approximation and that will counteract the dynamic potential that leads to these time-dependent resonances. Maitra and co-workers have shown that this requires memory-dependence in the XC functional. Our work here shows that the XC functional must also uncouple single-electron transitions in order to give two time-independent resonances. Since almost all practical applications of RT-TDDFT currently remain within the adiabatic approximation, this work provides a needed explanation of the RT-TDDFT peak-shifting observed when perturbing the density from the ground state reference.

■ ASSOCIATED CONTENT

Supporting Information

The Supporting Information is available free of charge on the ACS Publications website at DOI: 10.1021/acs.jctc.5b00559.

Field parameters for all simulations; RT-TDDFT MO populations of HeH^+, H_2 with high-intensity fields, and H_2 with 6-31G basis; TDCI coefficients of HeH^+; and energy analysis of H_2 in the minimal basis (PDF)

■ AUTHOR INFORMATION

Corresponding Author

*E-mail: cisborn@ucmerced.edu.

Notes

The authors declare no competing financial interest.

■ ACKNOWLEDGMENTS

C.M.I. is grateful for financial support from the Hellman Faculty Fund and from the American Chemical Society Petroleum Research Fund (53674-DNI6).

■ REFERENCES

(1) Caricato, M.; Trucks, G. W.; Frisch, M. J.; Wiberg, K. B. Electronic Transition Energies: A Study of the Performance of a Large Range of Single Reference Density Functional and Wave Function Methods on Valence and Rydberg States Compared to Experiment. *J. Chem. Theory Comput.* **2010**, *6*, 370−383.

(2) Jacquemin, D.; Mennucci, B.; Adamo, C. Excited-State Calculations with TD-DFT: From Benchmarks to Simulations in Complex Environments. *Phys. Chem. Chem. Phys.* **2011**, *13*, 16987−16998.

DOI: 10.1021/acs.jctc.5b00559
J. Chem. Theory Comput. 2015, 11, 4791−4802

(3) Leang, S. S.; Zahariev, F.; Gordon, M. S. Benchmarking the Performance of Time-Dependent Density Functional Methods. *J. Chem. Phys.* **2012**, *136*, 104101.
(4) Laurent, A. D.; Jacquemin, D. TD-DFT Benchmarks: A Review. *Int. J. Quantum Chem.* **2013**, *113*, 2019−2039.
(5) Casida, M. E. Time-Dependent Density Functional Response Theory for Molecules. In *Recent Advances in Density Functional Methods*; Chong, D. P., Ed.; Recent Advances in Computational Chemistry; World Scientific: 1995; Vol. Vol. *1*, pp 155−192.
(6) Nazeeruddin, M. K.; Angelis, F. De; Fantacci, S.; Selloni, A.; Viscardi, G.; Liska, P.; Ito, S.; Takeru, B.; Chimica, D.; Uni, V.; Elce, V. Combined Experimental and DFT-TDDFT Computational Study of Photoelectrochemical Cell Ruthenium Sensitizers. *J. Am. Chem. Soc.* **2005**, *127*, 16835−16847.
(7) Furche, F.; Ahlrichs, R.; Wachsmann, C.; Weber, E.; Sobanski, A.; Vo, F. Circular Dichroism of Helicenes Investigated by Time-Dependent Density Functional Theory. *J. Am. Chem. Soc.* **2000**, *122*, 1717−1724.
(8) Aikens, C. M.; Li, S.; Schatz, G. C. From Discrete Electronic States to Plasmons: TDDFT Optical Absorption Properties of Ag_n (n = 10, 20, 35, 56, 84, 120) Tetrahedral Clusters. *J. Phys. Chem. C* **2008**, *112*, 11272−11279.
(9) Tozer, D. J.; Handy, N. C. On the Determination of Excitation Energies Using Density Functional Theory. *Phys. Chem. Chem. Phys.* **2000**, *2*, 2117−2121.
(10) Dreuw, A.; Head-Gordon, M. Single-Reference Ab Initio Methods for the Calculation of Excited States of Large Molecules. *Chem. Rev.* **2005**, *105*, 4009−4037.
(11) Burke, K. Perspective on Density Functional Theory. *J. Chem. Phys.* **2012**, *136*, 150901.
(12) *Time-Dependent Density Functional Theory*; Marques, M. A. L.; Ullrich, C. A.; Nogueira, F.; Rubio, A.; Burke, K.; Gross, E. K. U., Eds.; Lecture Notes in Physics; Springer: Berlin, Heidelberg, 2006; Vol. *706*.
(13) Li, X.; Smith, S. M.; Markevitch, A. N.; Romanov, D. A.; Levis, R. J.; Schlegel, H. B. A Time-Dependent Hartree-Fock Approach for Studying the Electronic Optical Response of Molecules in Intense Fields. *Phys. Chem. Chem. Phys.* **2005**, *7*, 233−239.
(14) Yabana, K.; Sugiyama, T.; Shinohara, Y.; Otobe, T.; Bertsch, G. F. Time-Dependent Density Functional Theory for Strong Electromagnetic Fields in Crystalline Solids. *Phys. Rev. B: Condens. Matter Mater. Phys.* **2012**, *85*, 045134.
(15) Fuks, J. I.; Helbig, N.; Tokatly, I. V.; Rubio, A. Nonlinear Phenomena in Time-Dependent Density-Functional Theory: What Rabi Oscillations Can Teach Us. *Phys. Rev. B: Condens. Matter Mater. Phys.* **2011**, *84*, 075107.
(16) Lopata, K.; Govind, N. Modeling Fast Electron Dynamics with Real-Time Time-Dependent Density Functional Theory: Application to Small Molecules and Chromophores. *J. Chem. Theory Comput.* **2011**, *7*, 1344−1355.
(17) Maitra, N. T.; Burke, K. Demonstration of Initial-State Dependence in Time-Dependent Density-Functional Theory. *Phys. Rev. A: At., Mol., Opt. Phys.* **2001**, *63*, 042501.
(18) Maitra, N.; Burke, K.; Woodward, C. Memory in Time-Dependent Density Functional Theory. *Phys. Rev. Lett.* **2002**, *89*, 023002.
(19) Hessler, P.; Maitra, N. T.; Burke, K. Correlation in Time-Dependent Density-Functional Theory. *J. Chem. Phys.* **2002**, *117*, 72−81.
(20) Kurzweil, Y.; Baer, R. Time-Dependent Exchange-Correlation Current Density Functionals with Memory. *J. Chem. Phys.* **2004**, *121*, 8731−8741.
(21) Baer, R.; Kurzweil, Y.; Cederbaum, L. S. Time-Dependent Density Functional Theory for Nonadiabatic Processes. *Isr. J. Chem.* **2005**, *45*, 161−170.
(22) Schirmer, J.; Dreuw, A. Critique of the Foundations of Time-Dependent Density-Functional Theory. *Phys. Rev. A: At., Mol., Opt. Phys.* **2007**, *75*, 022513.
(23) Maitra, N.; van Leeuwen, R.; Burke, K. Comment on "Critique of the Foundations of Time-Dependent Density-Functional Theory". *Phys. Rev. A: At., Mol., Opt. Phys.* **2008**, *78*, 056501.
(24) Chapman, C. T.; Liang, W.; Li, X. Ultrafast Coherent Electron−Hole Separation Dynamics in a Fullerene Derivative. *J. Phys. Chem. Lett.* **2011**, *2*, 1189−1192.
(25) Petrone, A.; Lingerfelt, D. B.; Rega, N.; Li, X. From Charge-Transfer to a Charge-Separated State: A Perspective from the Real-Time TDDFT Excitonic Dynamics. *Phys. Chem. Chem. Phys.* **2014**, *16*, 24457−24465.
(26) Meng, S.; Kaxiras, E. Electron and Hole Dynamics in Dye-Sensitized Solar Cells: Influencing Factors and Systematic Trends. *Nano Lett.* **2010**, *10*, 1238−1247.
(27) Cheng, C.-L.; Evans, J. S.; Van Voorhis, T. Simulating Molecular Conductance Using Real-Time Density Functional Theory. *Phys. Rev. B: Condens. Matter Mater. Phys.* **2006**, *74*, 155112.
(28) Ding, F.; Guidez, E. B.; Aikens, C. M.; Li, X. Quantum Coherent Plasmon in Silver Nanowires: A Real-Time TDDFT Study. *J. Chem. Phys.* **2014**, *140*, 244705.
(29) Chen, H.; Ratner, M. A.; Schatz, G. C. Time-Dependent Theory of the Rate of Photo-Induced Electron Transfer. *J. Phys. Chem. C* **2011**, *115*, 18810−18821.
(30) Bende, A.; Toşa, V. Modeling Laser Induced Molecule Excitation Using Real-Time Time-Dependent Density Functional Theory: Application to 5- and 6-Benzyluracil. *Phys. Chem. Chem. Phys.* **2015**, *17*, 5861−5871.
(31) Fischer, S. A.; Cramer, C. J.; Govind, N. Excited State Absorption from Real-Time Time-Dependent Density Functional Theory. *J. Chem. Theory Comput.* **2015**, *11*, 4294.
(32) Isborn, C. M.; Li, X.; Tully, J. C. Time-Dependent Density Functional Theory Ehrenfest Dynamics: Collisions between Atomic Oxygen and Graphite Clusters. *J. Chem. Phys.* **2007**, *126*, 134307.
(33) Liang, W.; Isborn, C. M.; Li, X. Laser-Controlled Dissociation of C2H2(2+): Ehrenfest Dynamics Using Time-Dependent Density Functional Theory. *J. Phys. Chem. A* **2009**, *113*, 3463−3469.
(34) Liang, W.; Isborn, C. M.; Lindsay, A.; Li, X.; Smith, S. M.; Levis, R. J. Time-Dependent Density Functional Theory Calculations of Ehrenfest Dynamics of Laser Controlled Dissociation of NO+: Pulse Length and Sequential Multiple Single-Photon Processes. *J. Phys. Chem. A* **2010**, *114*, 6201−6206.
(35) Takimoto, Y.; Isborn, C. M.; Eichinger, B. E.; Rehr, J. J.; Robinson, B. H. Frequency and Solvent Dependence of Nonlinear Optical Properties of Molecules †. *J. Phys. Chem. C* **2008**, *112*, 8016−8021.
(36) Chapman, C. T.; Liang, W.; Li, X. Solvent Effects on Intramolecular Charge Transfer Dynamics in a Fullerene Derivative. *J. Phys. Chem. A* **2013**, *117*, 2687−2691.
(37) Chen, H.; Ratner, M. A.; Schatz, G. C. QM/MM Study of Photoinduced Reduction of a Tetrahedral Ag 20 + Cluster by a Ag Atom. *J. Phys. Chem. C* **2014**, *118*, 1755−1762.
(38) Morzan, U. N.; Ramírez, F. F.; Oviedo, M. B.; Sánchez, C. G.; Scherlis, D. A.; Lebrero, M. C. G. Electron Dynamics in Complex Environments with Real-Time Time Dependent Density Functional Theory in a QM-MM Framework. *J. Chem. Phys.* **2014**, *140*, 164105.
(39) Schlegel, H. B.; Smith, S. M.; Li, X. Electronic Optical Response of Molecules in Intense Fields: Comparison of TD-HF, TD-CIS, and TD-CIS(D) Approaches. *J. Chem. Phys.* **2007**, *126*, 244110.
(40) Thiele, M.; Kummel, S. Photoabsorption Spectra from Adiabatically Exact Time-Dependent Density-Functional Theory in Real Time. *Phys. Chem. Chem. Phys.* **2009**, *11*, 4631−4639.
(41) Raghunathan, S.; Nest, M. Critical Examination of Explicitly Time-Dependent Density Functional Theory for Coherent Control of Dipole Switching. *J. Chem. Theory Comput.* **2011**, *7*, 2492−2497.
(42) Takimoto, Y.; Vila, F. D.; Rehr, J. J. Real-Time Time-Dependent Density Functional Theory Approach for Frequency-Dependent Nonlinear Optical Response in Photonic Molecules. *J. Chem. Phys.* **2007**, *127*, 154114.
(43) Tussupbayev, S.; Govind, N.; Lopata, K.; Cramer, C. J. Comparison of Real-Time and Linear-Response Time-Dependent

DOI: 10.1021/acs.jctc.5b00559
J. Chem. Theory Comput. 2015, 11, 4791−4802

Density Functional Theories for Molecular Chromophores Ranging from Sparse to High Densities of States. *J. Chem. Theory Comput.* **2015**, *11*, 1102−1109.
(44) Fuks, J. I.; Luo, K.; Sandoval, E. D.; Maitra, N. T. Time-Resolved Spectroscopy in Time-Dependent Density Functional Theory: An Exact Condition. *Phys. Rev. Lett.* **2015**, *114*, 183002.
(45) Ruggenthaler, M.; Bauer, D. Rabi Oscillations and Few-Level Approximations in Time-Dependent Density Functional Theory. *Phys. Rev. Lett.* **2009**, *102*, 233001.
(46) Elliott, P.; Fuks, J. I.; Rubio, A.; Maitra, N. T. Universal Dynamical Steps in the Exact Time-Dependent Exchange-Correlation Potential. *Phys. Rev. Lett.* **2012**, *109*, 266404.
(47) Fuks, J. I.; Elliott, P.; Rubio, a.; Maitra, N. T. Dynamics of Charge-Transfer Processes with Time-Dependent Density Functional Theory. *J. Phys. Chem. Lett.* **2013**, *4*, 735−739.
(48) Isborn, C. M.; Li, X. Modeling the Doubly Excited State with Time-Dependent Hartree-Fock and Density Functional Theories. *J. Chem. Phys.* **2008**, *129*, 204107.
(49) Habenicht, B. F.; Tani, N. P.; Provorse, M. R.; Isborn, C. M. Two-Electron Rabi Oscillations in Real-Time Time-Dependent Density-Functional Theory. *J. Chem. Phys.* **2014**, *141*, 184112.
(50) Padmanaban, R.; Nest, M. Origin of Electronic Structure and Time-Dependent State Averaging in the Multi-Configuration Time-Dependent Hartree−Fock Approach to Electron Dynamics. *Chem. Phys. Lett.* **2008**, *463*, 263−266.
(51) Raghunathan, S.; Nest, M. The Lack of Resonance Problem in Coherent Control with Real-Time Time-Dependent Density Functional Theory. *J. Chem. Theory Comput.* **2012**, *8*, 806−809.
(52) Raghunathan, S.; Nest, M. Coherent Control and Time-Dependent Density Functional Theory: Towards Creation of Wave Packets by Ultrashort Laser Pulses. *J. Chem. Phys.* **2012**, *136*, 064104.
(53) Raghunathan, S.; Nest, M. Limits of the Creation of Electronic Wave Packets Using Time-Dependent Density Functional Theory. *J. Phys. Chem. A* **2012**, *116*, 8490−8493.
(54) De Giovannini, U.; Brunetto, G.; Castro, A.; Walkenhorst, J.; Rubio, A. Simulating Pump-Probe Photoelectron and Absorption Spectroscopy on the Attosecond Timescale with Time-Dependent Density Functional Theory. *ChemPhysChem* **2013**, *14*, 1363−1376.
(55) Becke, A. D. Density-Functional Thermochemistry. III. The Role of Exact Exchange. *J. Chem. Phys.* **1993**, *98*, 5648.
(56) Lee, C.; Yang, W.; Parr, R. G. Development of the Colle-Salvetti Correlation-Energy Formula into a Functional of the Electron Density. *Phys. Rev. B: Condens. Matter Mater. Phys.* **1988**, *37*, 785−789.
(57) Frisch, M. J.; Trucks, G. W.; Schlegel, H. B.; Scuseria, G. E.; Robb, M. A.; Cheeseman, J. R.; Scalmani, G.; Barone, V.; Mennucci, B.; Petersson, G. A.; Nakatsuji, H.; Caricato, M.; Li, X.; Hratchian, H. P.; Izmaylov, A. F.; Bloino, J.; Zheng, G.; Sonnenberg, J. L.; Liang, W.; Hada, M.; Ehara, M.; Toyota, K.; Fukuda, R.; Hasegawa, J.; Ishida, M.; Nakajima, T.; Honda, Y.; Kitao, O.; Nakai, H.; Vreven, T.; Montgomery, J. A., Jr.; Peralta, J. E.; Ogliaro, F.; Bearpark, M.; Heyd, J. J.; Brothers, E.; Kudin, K. N.; Staroverov, V. N.; Keith, T.; Kobayashi, R.; Normand, J.; Raghavachari, K.; Rendell, A.; Burant, J. C.; Iyengar, S. S.; Tomasi, J.; Cossi, M.; Rega, N.; Millam, M. J.; Klene, M.; Knox, J. E.; Cross, J. B.; Bakken, V.; Adamo, C.; Jaramillo, J.; Gomperts, R.; Stratmann, R. E.; Yazyev, O.; Austin, A. J.; Cammi, R.; Pomelli, C.; Ochterski, J. W.; Martin, R. L.; Morokuma, K.; Zakrzewski, V. G.; Voth, G. A.; Salvador, P.; Dannenberg, J. J.; Dapprich, S.; Parandekar, P. V.; Mayhall, N. J.; Daniels, A. D.; Farkas, Ö.; Foresman, J. B.; Ortiz, J. V.; Cioslowski, J.; Fox, D. J. *Gaussian Development Version, Revision H.32+*; 2010.
(58) Handy, N. C.; Schaefer, H. F. On the Evaluation of Analytic Energy Derivatives for Correlated Wave Functions. *J. Chem. Phys.* **1984**, *81*, 5031.
(59) Furche, F.; Ahlrichs, R. Adiabatic Time-Dependent Density Functional Methods for Excited State Properties. *J. Chem. Phys.* **2002**, *117*, 7433.

DOI: 10.1021/acs.jctc.5b00559
J. Chem. Theory Comput. 2015, 11, 4791−4802